Overview of the CALIPSO Mission and CALIOP Data Processing Algorithms

DAVID M. WINKER, MARK A. VAUGHAN, ALI OMAR, YONGXIANG HU, AND KATHLEEN A. POWELL

NASA Langley Research Center, Hampton, Virginia

ZHAOYAN LIU

National Institute of Aerospace, Hampton, Virginia

WILLIAM H. HUNT

Science Systems and Applications Inc., Hampton, Virginia

STUART A. YOUNG

CSIRO Marine and Atmospheric Research, Aspendale, Victoria, Australia

(Manuscript received 13 January 2009, in final form 16 March 2009)

ABSTRACT

The Cloud-Aerosol Lidar with Orthogonal Polarization (CALIOP) is a two-wavelength polarization lidar that performs global profiling of aerosols and clouds in the troposphere and lower stratosphere. CALIOP is the primary instrument on the Cloud-Aerosol Lidar and Infrared Pathfinder Satellite Observations (CALIPSO) satellite, which has flown in formation with the NASA A-train constellation of satellites since May 2006. The global, multiyear dataset obtained from CALIOP provides a new view of the earth's atmosphere and will lead to an improved understanding of the role of aerosols and clouds in the climate system. A suite of algorithms has been developed to identify aerosol and cloud layers and to retrieve a variety of optical and microphysical properties. CALIOP represents a significant advance over previous space lidars, and the algorithms that have been developed have many innovative aspects to take advantage of its capabilities. This paper provides a brief overview of the CALIPSO mission, the CALIOP instrument and data products, and an overview of the algorithms used to produce these data products.

1. Introduction

Aerosols and clouds have important impacts on the earth's climate through their effects on the radiation budget and the role they play in the water cycle. Clouds reflect sunlight back to space and trap outgoing thermal radiation emitted by the earth's surface, modulating the radiative balance of the earth–atmosphere system. The net effect of these competing cooling and warming effects depends on the altitude of the cloud layers and their multilayer structures. Aerosols also scatter sunlight back to space, producing cooling at the earth's surface. Absorbing aerosols warm the atmosphere, which can influence the profile of atmospheric stability and suppress cloud formation. Because cloud droplets form on aerosol particles, changes in aerosol concentration and properties can alter cloud properties and precipitation. There are many sources of aerosols—both natural and resulting from human activities—with widely varying distribution and properties. The largest uncertainties in our ability to predict future climate change are associated with uncertainties in the distribution and properties of aerosols and clouds and their interactions, as well as with limitations in how aerosols and clouds are represented in global climate models (Solomon et al. 2007).

Corresponding author address: David M. Winker, NASA Langley Research Center, MS 475, Hampton, VA 23681.
E-mail: david.m.winker@nasa.gov

DOI: 10.1175/2009JTECHA1281.1

The Cloud-Aerosol Lidar and Infrared Pathfinder Satellite Observations (CALIPSO) mission was developed as part of the National Aeronautics and Space Administration (NASA) Earth System Science Pathfinder (ESSP) program in collaboration with Centre National d'Études Spatiales (CNES), the French space agency, with the goal of filling existing gaps in our ability to observe the global distribution and properties of aerosols and clouds (Winker et al. 2003). CALIPSO was launched together with the CloudSat satellite in April 2006 and is now flying in formation with the A-train constellation of satellites (Stephens et al. 2002). The satellites of the A-train are in a 705-km sun-synchronous polar orbit, giving a 16-day repeat cycle, with an equator-crossing time of about 1330 local solar time. The orbit inclination of 98.2° provides global coverage from CALIPSO between 82°N and 82°S. The CALIPSO orbit is controlled to keep cross-track errors with respect to the 16-day grid less than ±10 km. Careful control of the CALIPSO orbit with respect to the other A-train satellites ensures the acquisition of collocated near-simultaneous measurements.

The primary instrument carried on the CALIPSO satellite is the Cloud-Aerosol Lidar with Orthogonal Polarization (CALIOP), a near-nadir viewing two-wavelength polarization-sensitive lidar. CALIOP is the first polarization lidar to provide global atmospheric measurements and as such offers new observational capabilities to the international scientific community. CALIPSO also carries two passive sensors. The wide field camera is a charge-coupled device (CCD)-based visible sensor with a spatial resolution of 125 m for pixels within 2.5 km of the subsatellite point and 1000 m for the remaining pixels in the swath extending to 30 km on either side. The infrared imaging radiometer is a three-channel instrument with a spatial resolution of 1 km and a swath of 61 km. Both swaths are centered on the lidar footprint to provide a view of the atmosphere surrounding the lidar curtain.

Aerosols are now being observed from space using a variety of passive techniques relying on scattered sunlight, with some measurement series extending more than 20 yr (King et al. 1999). Remote sensing of aerosol properties is difficult, however, owing to the great variability in aerosol sources, distribution and properties, effects of surface reflectance, and interference from clouds. Active sensing of aerosols with lidar offers unique capabilities which are complementary to those of passive techniques. Lidar is the only technique giving high-resolution profiles of aerosols, and it is able to observe aerosol above bright surfaces, such as deserts and snow, and above bright clouds. Because lidar provides its own illumination, aerosol can be observed over the full globe—night as well as day—yielding a more complete dataset for the validation of regional and global aerosol models.

There are also many limitations in sensing clouds using passive satellite techniques. Passive satellite sensors have difficulty retrieving the height of semitransparent clouds and often miss optically thin clouds entirely. Roughly half of all cloud systems are multilayered (Hahn et al. 1990) and the net radiative effect of cloud depends strongly on the multilayer structure, yet passive sensors have difficulty retrieving more than a single effective layer. Lidar is able to penetrate high optically thin cloud and profile a large fraction of the atmosphere. There are also limitations in current cloud ice–water phase retrievals from passive satellite sensors. CALIOP provides a vertically resolved measurement of ice–water phase through measurements of the depolarization of the lidar backscatter signal.

CALIPSO was originally proposed to fly in formation with the Earth Observing System (EOS) *Aqua* satellite to provide profile information to supplement observations of aerosol, cloud, and radiative fluxes being acquired by the Moderate Resolution Imaging Spectroradiometer (MODIS) and Clouds and the Earth's Radiant Energy System (CERES) instruments (Winker et al. 2003). This initial concept of CALIPSO and *Aqua* flying in formation has grown into a formation of 5 satellites [CALIPSO, CloudSat, *Aqua*, *Aura*, and Polarization and Anisotrophy of Reflectances for Atmospheric Sciences Coupled with Observations from a Lidar (PARASOL); Stephens et al. 2002], which offers numerous additional measurement synergies with CALIPSO [e.g., cloud profile measurements from CloudSat and aerosol measurements from the Ozone Monitoring Instrument (OMI; on board *Aura*) and PARASOL]. The A-train is soon to be augmented by the Glory satellite (Mishchenko et al. 2007), providing additional aerosol measurements using multiangle–polarization techniques. Nevertheless, the original measurement requirements defined for CALIOP (see Table 1) constitute a unique and important dataset and form the core of the CALIOP data products.

This overview paper provides a brief summary of the CALIPSO mission, the CALIOP instrument and data products, and the algorithms used to produce them. Few lidars have flown in space and none with the capabilities of CALIOP. Therefore, many aspects of the CALIOP algorithms are unique. We describe the conceptual basis of the CALIOP retrieval approach, relations between the various level 2 algorithms, and discuss basic characteristics of the data products. Details of the CALIOP instrument and algorithms can be found in the companion papers in this special issue. Additional details can be found in the CALIPSO algorithm theoretical basis documents (ATBDs; available online at http://www-calipso.larc.nasa.gov/resources/project_documentation.php).

TABLE 1. Primary CALIOP science products and uncertainties.

Data product	Measurement capabilities and uncertainties	
	Aerosols	Clouds
Height	For layers with $\tau > 0.005$	For layers with $\tau > 0.01$
Thickness	For layers with $\tau < 3$	For layers with $\tau < 5$
Extinction profile and optical depth τ	40%*	Within a factor of 2 for $\tau < 5$**
Ice–water phase		Layer by layer

* For highest layer.
** For constrained retrievals.

2. The CALIOP instrument

CALIOP is built around a solid-state neodymium-doped yttrium aluminum garnet (Nd:YAG) laser that produces simultaneous coaligned pulses at 1064 and 532 nm. The laser generates optical pulses that are about 20 ns long (~6 m) with nominally 110 mJ of energy at each of the two wavelengths. Energy monitors measure the output pulse energy at each wavelength. A beam expander reduces the angular divergence of the transmitted laser beam to produce a beam diameter of ~70 m at the earth's surface. The laser pulse repetition frequency of 20.16 Hz produces footprints every 335 m along the ground. The instrument operates continuously, acquiring 1.7 million laser shots every 24 h and providing observations during both day and night portions of the orbit.

Figure 1 provides a functional description of CALIOP. Backscatter signals are collected by a 1-m diameter telescope. The receiver footprint diameter is 90 m at the ground. To reduce the solar background, an etalon and an interference filter provide a passband of 35 pm for the 532-nm channel, whereas an interference filter alone is sufficient for the 1064-nm channel. The outgoing 532-nm pulses are linearly polarized with polarization purity greater than 99%. A polarization beamsplitter separates the components of the 532-nm return signal polarized parallel and perpendicular to the plane of the outgoing beam, which are detected by two photomultiplier detectors. A pseudodepolarizer located ahead of the beamsplitter can be moved into the beam for relative calibration of the two 532-nm channels.

CALIOP is required to accurately measure signal returns from the aerosol-free region between 30 and 35 km as well as the strongest cloud returns. Therefore, it has been designed so that the linear dynamic range encompasses the full range of molecular, aerosol, and cloud backscattering encountered in the atmosphere, which spans 5 orders of magnitude. Photomultiplier tubes (PMTs) were chosen for detection at 532 nm because they provide a very large linear dynamic range, very low dark current, and reasonable quantum efficiency. An avalanche photodiode is used in the 1064-nm channel. Dual 14-bit digitizers on each channel provide the required 22-bit dynamic range. All detectors are operated in analog mode, although the 532-nm channels are sensitive enough to measure single photon events.

The fundamental sampling resolution of the lidar is 30 m vertical and 335 m horizontal, determined by the receiver electrical bandwidth and the laser pulse repetition rate. The instrument measures the background illumination of each profile while the laser pulse is at altitudes between 112 and 97 km, a region where the atmospheric return signals are negligible. These signals are averaged to characterize the solar background illumination. Only the samples acquired below 40 km for the 532-nm channel and below 30 km for the 1064-nm channel are downlinked as profile data. Realizing that spatial scales of atmospheric variability tend to increase with altitude, data above an altitude of 8.2 km are averaged vertically and horizontally on board the satellite before downlinking (according to the scheme shown in Table 2) to reduce the telemetry bandwidth required. Further details on the instrument and data acquisition are given in Hunt et al. (2009), and initial evaluations of on-orbit performance can be found in Winker et al. (2007) and McGill et al. (2007).

CALIPSO flies in a near-nadir attitude so that the CALIOP footprints nominally fall on the satellite groundtrack. Prior to November 2007, the satellite attitude was controlled to point CALIOP 0.3° from geodetic nadir in the forward along-track direction. This small off-nadir angle avoids strong specular lidar returns from still water (e.g., ponds and rivers). In November 2007, the nadir angle was increased to 3° to reduce specular returns from clouds containing horizontally oriented ice crystals, which contribute to retrieval uncertainties.

Two other space lidars have provided atmospheric measurements prior to CALIOP. The Lidar In-space Technology Experiment (LITE) was a concept demonstration experiment that flew on the Space Transportation System (STS)-64 mission in September 1994 (Winker et al. 1996). LITE was the first lidar to observe the atmosphere from orbit and demonstrated the potential of satellite lidar for observing cloud and aerosol.

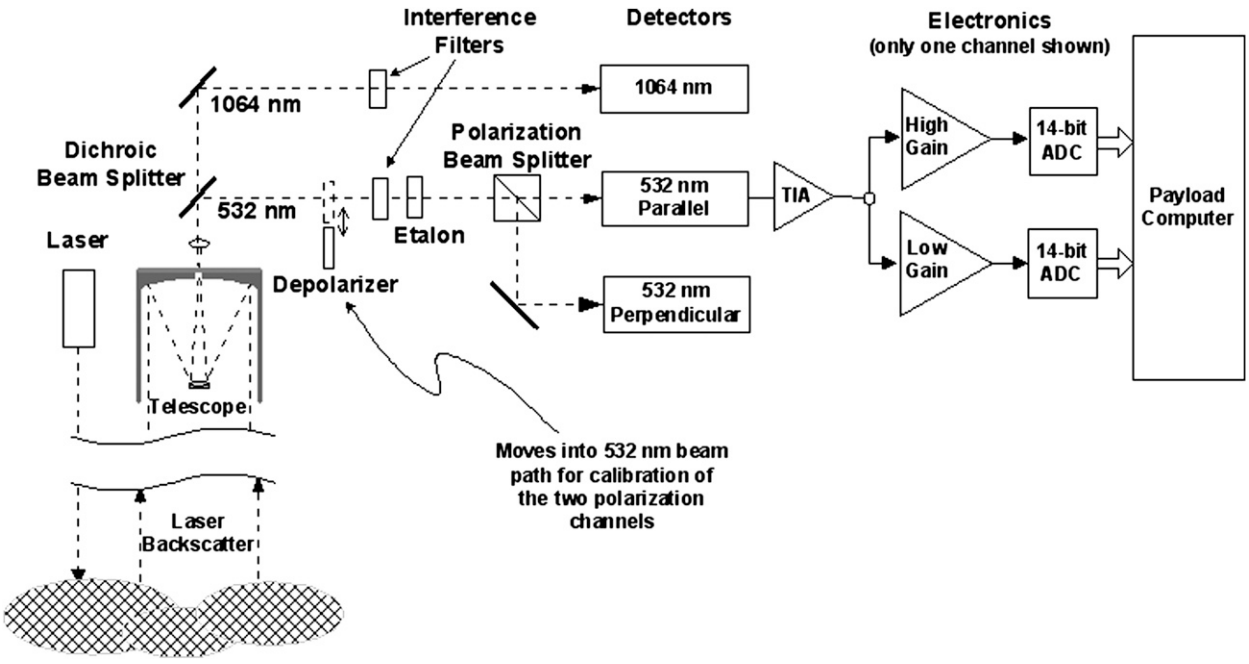

FIG. 1. Block diagram of the CALIOP instrument.

LITE had high sensitivity because of its low orbit and high laser pulse energies, but the receiver had limited dynamic range. Cloud signals were saturated at the high detector gains used to observe aerosol. When gains were reduced to acquire unsaturated cloud signals, aerosol measurements were suboptimal. The Geoscience Laser Altimeter System (GLAS) flying on the Ice, Cloud, and Land Elevation Satellite (ICESat) was primarily intended to provide high-resolution ice sheet altimetry but also has an atmospheric profiling capability (Abshire et al. 2005). The CALIOP 532-nm channel has roughly similar sensitivity to the GLAS 532-nm channel during the early part of the ICESat mission, but the GLAS 532-nm channel has limited dynamic range. The GLAS 1064-nm channel has lower sensitivity than the CALIOP 1064-nm channel. Neither of these instruments measured the polarization of the lidar backscatter signal. Algorithm development for CALIOP benefited from the experience gained from these earlier missions, but the enhanced capabilities of the CALIOP instrument presented a challenge to develop a new generation of retrieval algorithms to make full use of the measurements.

3. Overview of the data processing system

The CALIPSO data downlink and data processing systems were designed to meet processing and archive requirements appropriate for climate research. Current data turnaround time for the acquisition, processing, and archival of nominal science data products is about 5 days. Using an approximate calibration, a limited set of "expedited" products is also produced, with a turnaround time of about 24 h. All CALIPSO payload science data are downlinked once per day to an X-band ground station in Alaska. The X-band telemetry also includes payload health and status data. The telemetry data are processed to level 0 data and sent to the Atmospheric Sciences Data Center (ASDC) located at NASA Langley Research Center in Hampton, Virginia. Further processing, archiving, and distribution of data from all three instruments are performed by ASDC. Figure 2 shows the portion of the ASDC data processing flow for CALIOP. Each day, approximately 3.5 GB of level 0 instrument science data are received from which 20 GB of CALIOP level 1 and level 2 products are produced. A number of ancillary datasets are required by the nominal processing flow. Gridded meteorological

TABLE 2. Spatial resolution of downlinked data from CALIOP.

Altitude range (km)	Horizontal resolution (km)	532-nm vertical resolution (m)	1064-nm vertical resolution (m)
30.1–40.0	5.0	300	—
20.2–30.1	1.67	180	180
8.2–20.2	1.0	60	60
−0.5 to 8.2	0.33	30	60
−2.0 to −0.5	0.33	300	300

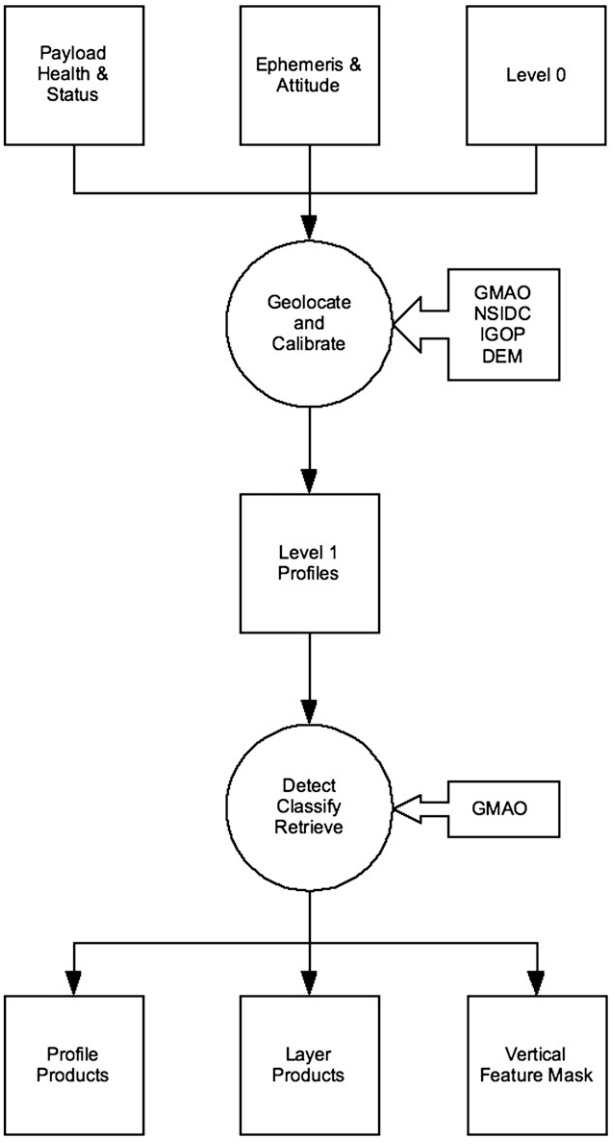

FIG. 2. CALIOP data flow within the CALIPSO data processing system.

and ozone fields from the NASA Global Modeling and Assimilation Office (GMAO), satellite attitude and post-processed ephemeris data from CNES, and snow and ice data from the National Snow and Ice Data Center (NSIDC) are delivered daily. Several static datasets are also used: the International Geosphere-Biosphere Programme (IGBP) surface vegetation cover map and the digital elevation map (DEM) built into the NASA Earth Observing System Data and Information System (EOSDIS) Core System Toolkit. When all necessary data products have been delivered, a production script automatically initiates level 1 and then level 2 data processing. Table 3 lists the primary CALIOP data products and their contents.

Release history

CALIOP version 1 data were released in December 2006. This release consisted of level 1B data and a subset of level 2 layer products. Initial version 1 algorithms were developed prior to launch, using data from LITE and from the Cloud Physics Lidar (McGill et al. 2002).

Version 2 data products were released in January 2008 and included, for the first time, aerosol and cloud profile products and results from extinction retrievals. Daytime calibration, layer detection, and layer classification algorithms were all significantly improved in version 2. Version 2 also contains aerosol type, cloud ice–water phase, and profile products for the first time.

CALIOP level 1b data consist of geolocated profiles of calibrated lidar return signals (normalized attenuated backscatter) along with information on surface type, calibration and quality assurance, and a limited set of instrument status data. Three types of profiles are provided in the level 1B product: total backscatter (parallel plus perpendicular) at 532 and 1064 nm and the 532-nm perpendicular backscatter. The geolocation and calibration procedures are briefly described below.

There are three basic types of level 2 data products: layer products, profile products, and the vertical feature mask (VFM). Layer products provide layer-integrated or layer-averaged properties of detected aerosol and cloud layers. Profile products provide retrieved extinction and backscatter profiles within these layers. The data products are provided at various spatial resolutions. Because of the low signal-to-noise ratio (SNR) characteristic of lidar, especially satellite lidar, more averaging is required to detect and retrieve weakly scattering layers than strongly scattering layers. A multiscale detection and retrieval approach, described later, was adopted to mitigate the impact of low SNR. Because information on the spatial locations of cloud and aerosol layers is of fundamental importance, the VFM was developed to provide information on cloud and aerosol locations and types. The information in the VFM is derived from the layer products and interpolated onto a vertical grid at the resolution of the downlinked data (Table 2).

All data products—as well as the data products catalog, algorithm theoretical basis documents, and other documentation—are available from the Atmospheric Sciences Data Center at NASA Langley Research Center (available online at http://eosweb.larc.nasa.gov). Further description of the data products can be found in Vaughan et al. (2004) and online documentation.

4. Level 1 processing

Level 1 processing consists of three-dimensional geolocation followed by calibration. These are briefly described

TABLE 3. Product summary for CALIOP version 2 data.

Product	Primary parameters	Max alt (km)	Resolution	
			Vertical (m)	Horizontal (km)
Level 1B	532-nm, 532-nm perpendicular, and 1064-nm attenuated backscatter profiles	40	Variable (see Table 2)	
Cloud layer	Base and top height, optical depth, ice–water phase	20	30	1/3, 1, and 5
Aerosol layer	Base and top height, optical depth, aerosol type	30	30	5
Cloud profile	532-nm backscatter and extinction	20	60	5
Aerosol profile	532-nm/1064-nm backscatter and extinction	<20/20–30	120/360	40/40
Vertical feature mask	Cloud mask and ice–water phase; aerosol mask, aerosol type	30	Variable (see Table 2)	

in this section. Further details are given in Powell et al. (2009).

a. Geolocation

The geodetic location of each lidar footprint is determined using spacecraft attitude and ephemeris data. CALIPSO flies in a circular orbit whereas the earth is an oblate sphere, so the surface is further from the satellite at the poles than at the equator. As the satellite orbits the earth, the range to the surface changes continually and the range gates are automatically adjusted by the payload controller to keep the geoid surface within the digitized range (Hunt et al. 2009). During level 1 processing, the profiles are registered to a common altitude grid using postprocessed satellite ephemeris data. CALIOP profile altitudes are given as height above the earth geoid. Geolocation accuracies are roughly 50 m in the horizontal and 10 m in the vertical.

b. Calibration

CALIOP level 1 products contain profiles of attenuated backscatter, in units of $\mathrm{km}^{-1}\ \mathrm{sr}^{-1}$, for the 1064-nm channel, for the sum of the two 532-nm channels, and for the 532-nm perpendicular channel. Attenuated backscatter $\beta'(r)$ can be written as

$$\beta'(r) = [\beta_p(r) + \beta_m(r)]T^2(r_c, r),$$

where $\beta_p(r)$ and $\beta_m(r)$ represent the backscatter contributions from particles and from the molecular atmosphere at range r from the satellite, and $T^2(r_c, r)$ represents the two-way transmittance between a calibration region at r_c and range r. Calibration consists of converting the measured signal profile $P(r)$, in digitizer counts, to $\beta'(r)$:

$$\beta'(r) = \frac{r^2 P(r)}{CEG_A},$$

where C is the calibration coefficient, E is the measured laser pulse energy, and G_A is the electronic amplifier gain.

Nighttime profiles from the 532-nm parallel channel are calibrated by the standard lidar technique of normalizing the high-altitude return signal to a molecular model (Russell et al. 1979). If the aerosol concentration is negligible, the magnitude of the expected signal can be computed from profiles of molecular number density. At 532 nm, it is necessary to account for ozone absorption, which varies with altitude. The column absorption attenuates the measured backscatter signal in the lower troposphere by about 5%. Gridded GMAO meteorological data are interpolated to CALIOP measurement locations and the measured 532-nm parallel backscatter signal is calibrated by normalizing the observed signal to the predicted molecular signal in the region between 30 and 34 km. Aerosol content at these altitudes is assumed to be negligible for the period of the CALIPSO mission. An investigation indicates there may be a calibration bias of a few percent because of the background stratospheric aerosol, with a larger bias in the tropics than at higher latitudes (Thomason et al. 2007). Daytime background levels prevent this calibration technique from being applied to sunlit portions of the orbit, so daytime calibrations are interpolated from adjacent nighttime calibrations.

The relative gain of the two 532-nm channels is measured by inserting the pseudodepolarizer into the 532-nm beam path to put equal amounts of light onto each of the two 532-nm detectors, allowing the perpendicular channel to be calibrated relative to the parallel channel. The 532-nm parallel and perpendicular profiles are then summed to produce the 532-nm total attenuated backscatter profile, $\beta'(z) = \beta'_{\mathrm{par}}(z) + \beta'_{\mathrm{perp}}(z)$. The 1064-nm profile is calibrated relative to the 532-nm backscatter intensity using returns from cirrus clouds. The 1064-nm calibration algorithm assumes cirrus clouds are spectrally neutral backscatter targets. Although this is well established for extinction, spectral variability in backscatter has been observed to be larger than expected and studies are underway to better understand the variability (Vaughan et al. 2008). The end result of level 1 processing is calibrated profiles of 532-nm perpendicular

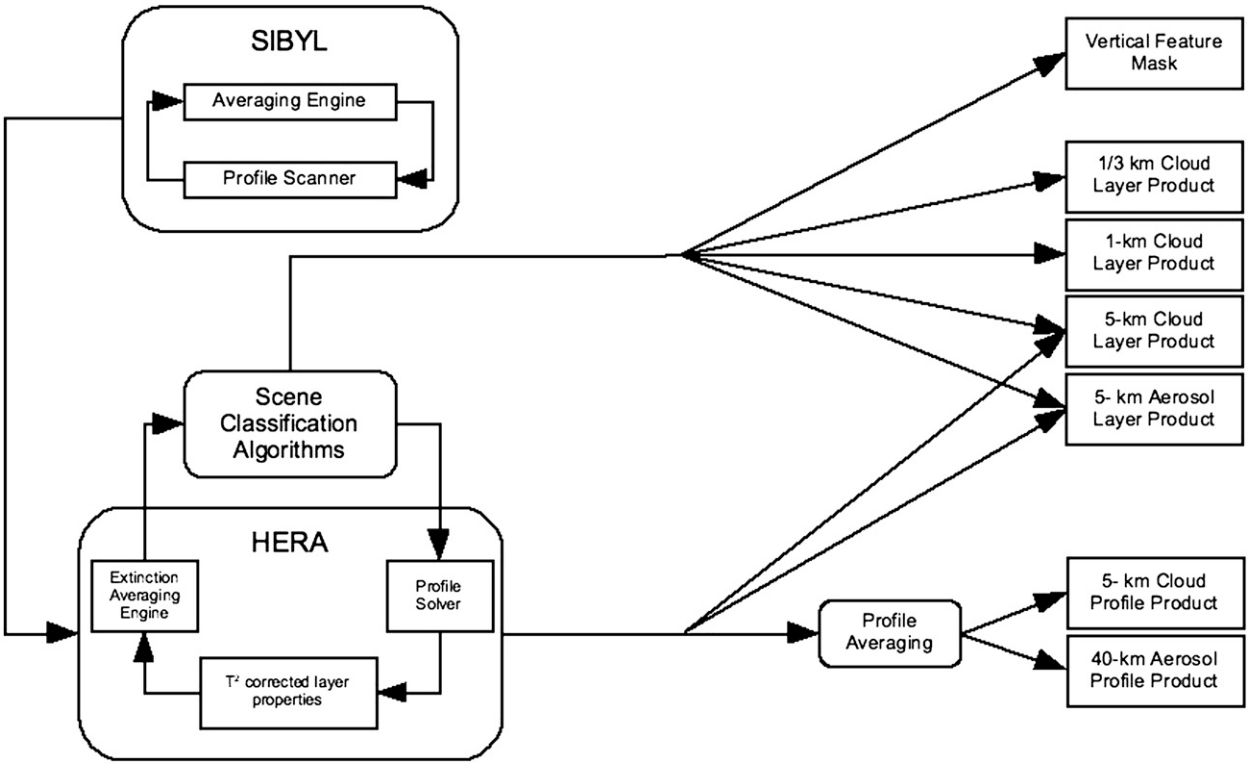

FIG. 3. Level 2 algorithm interfaces and data flow.

attenuated backscatter $\beta'_{\text{perp}}(z)$ and total attenuated backscatter $\beta(z)$ at 532 and 1064 nm.

5. Level 2 algorithm summary

The overall level 2 dataflow is shown schematically in Fig. 3. The level 2 processing involves three major steps. First, cloud and aerosol layers are identified by a set of algorithms referred to as the selective iterative boundary locator (SIBYL), applied to the 532-nm attenuated backscatter profiles. Second, a set of scene classification algorithms (SCA) classifies these layers by type. Using data from all three CALIOP channels, layers are identified as clouds or aerosols and the aerosol type and cloud ice–water phase are determined. Finally, profiles of particle backscatter and extinction coefficients are retrieved by the hybrid extinction retrieval algorithm (HERA). HERA performs retrievals within the layer boundaries identified by SIBYL. The retrieval requires a lidar ratio (the ratio of particle extinction to backscatter), which is either derived from the layer transmittance measured from clear-air returns above and below the layer or from a prescribed value provided by the SCA typing algorithm. If multiple cloud and/or aerosol layers are found in a column, scene classification and extinction retrieval are performed on the uppermost layer first. Classification and retrieval then proceed downward, layer by layer, so that scene classification of lower layers can be based on signals corrected for the attenuation of the overlying layers.

SNR is a primary consideration in designing retrieval algorithms for satellite lidar. The instrument is far from the atmosphere, laser pulse energy is limited by the available electrical power, and the footprint is moving across the earth's surface at nearly 7 km s^{-1}. The CALIOP SNR is necessarily much lower than for typical ground-based or airborne lidars. However, improving SNR by simple signal averaging can result in profiles averaged over inhomogeneous or broken cloud fields, producing results that are not representative of the radiative properties of the scene. Therefore, a substantial effort has been expended to develop a multiscale averaging scheme that improves SNR while preserving the homogeneity of the averaged profiles.

Figure 4 shows the estimated detection sensitivity of the CALIOP 532-nm channel with different amounts of horizontal averaging. Sensitivity is better at night than during day (somewhat better for cloud and substantially better for aerosol), and it improves with altitude because the magnitude of the molecular scattering decreases with altitude. Also shown are typical ranges of aerosol and cloud backscatter, which vary by many orders of

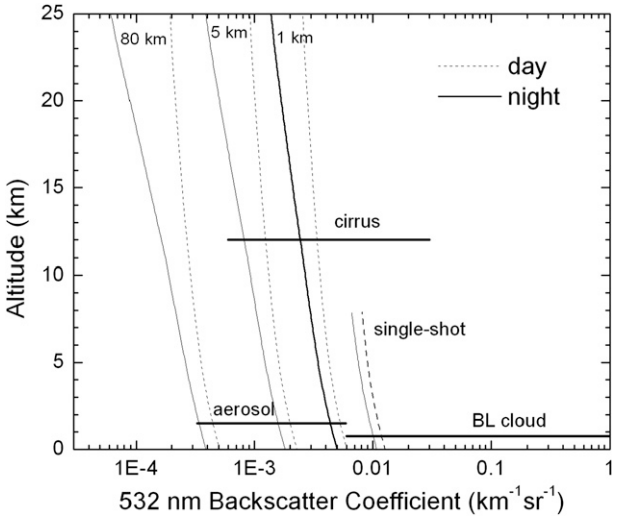

FIG. 4. Day (dashed) and night (solid) detection sensitivity in terms of minimum detectable particulate backscatter coefficient [$(\mathrm{km})^{-1}$ $(\mathrm{sr})^{-1}$] for 60-m vertical resolution. Single-shot sensitivity is compared to sensitivity with horizontal averaging over 1, 5, and 80 km. Horizontal lines indicate typical ranges of backscatter from cirrus and from aerosols and clouds in the atmospheric boundary layer.

magnitude. CALIOP has sufficient sensitivity to detect most boundary layer clouds from single shots, but horizontal averaging over a kilometer or more is required to detect most aerosol layers and weaker clouds. If extinction retrievals are attempted on profiles that have not been sufficiently averaged, the retrievals will be biased by signal noise, but the amount of averaging required depends on the scattering strength of the layer.

However, if the downlinked profiles are averaged enough to provide good SNR for aerosol retrievals, the spatial structure of cloud features will be lost and aerosols and clouds will sometimes be averaged together, resulting in biased retrievals. Therefore, a unique multiscale retrieval approach has been developed that attempts to achieve an optimum balance between SNR and spatial resolution. Strongly scattering clouds are detected and retrieved with little or no signal averaging, whereas significant signal averaging is performed to detect weakly scattering aerosols. This multiscale approach has driven the fundamental structure of the level 2 retrieval algorithms and output data products.

In this multiscale approach, the layer finding algorithm performs multiple passes through the data, scanning level 1 profiles with successively greater horizontal averaging. At each step, cloud and aerosol layers found at higher spatial resolutions (less averaging) are removed before further averaging. In production data processing, layer detection is performed on single shots and on profiles averaged over 1, 5, 20, and 80 km. The extinction retrieval algorithm constructs averaged profiles using the layer locations determined during the detection phase. After classification of each layer, extinction retrievals are performed on the layer at the resolution at which it was detected. This has the benefit of reducing the variability of SNR in the profiles that will be retrieved because weakly scattering layers are averaged more than strong ones.

a. Layer detection

The most fundamental data product from CALIOP is the height of cloud and aerosol layers. SIBYL consists of an algorithm to scan profiles to detect aerosol and cloud layers, and an algorithm to average profiles and remove detected layers from the profiles before further averaging (Fig. 3). Layers are identified in the atmospheric return signal as enhancements above the signal expected from the molecular background. Identification is performed using an adaptive thresholding technique applied to level one 532-nm profiles ($\beta'_{\mathrm{par}} + \beta'_{\mathrm{perp}}$), which generally provide better sensitivity than the 1064-nm channel. The level 1 profile is converted into a profile of attenuated scattering ratio $R'(z)$,

$$R'(z) = \frac{\beta'(r)}{\beta'_m(r)},$$

before the thresholding algorithm is applied. The profile of $\beta'_m(r)$ is estimated using gridded molecular and ozone number density profile data from the Goddard Earth Observing System Model, version 5 (GEOS-5) analysis product available from the NASA Goddard GMAO. The layer detection algorithm is adaptive in the sense that the magnitude of the threshold for layer identification is modified according to the characteristics of the signal. The threshold varies with altitude and is recomputed for each profile, because the noise envelope varies with altitude and during daytime can vary shot to shot because of variations in surface albedo. Beneath each layer, the magnitude of $R'(z)$ is corrected for the attenuation of the overlying layer; otherwise, aerosol layers located underneath higher aerosol or cloud layers tend to be missed. Further details of the detection algorithm and SIBYL are described in Vaughan et al. (2009).

b. Scene classification

The SCA is a set of algorithms that perform typing of the detected layers based on layer height and layer-integrated properties. SCA first determines if a layer is cloud or aerosol using the measured layer-mean attenuated backscatter at 532 nm and the layer-mean attenuated total color ratio χ':

$$\chi' = \frac{\langle \beta'_{1064} \rangle}{\langle \beta'_{532} \rangle},$$

where the averages are computed from layer top to base. If the layer is classified as aerosol, SCA uses a decision tree to classify the aerosol type. For layers classified as cloud, SCA determines the ice–water phase using layer-mean depolarization ratio and temperature information from the GMAO gridded analysis product.

1) Cloud–aerosol discrimination

Proper retrieval of aerosol and cloud properties requires first identifying and discriminating aerosols and clouds within the profile data. To avoid cloud contamination of aerosol retrievals, cloud returns must be identified and removed before profiles are averaged for aerosol retrievals. Because small-scale broken clouds are often found embedded in boundary layer aerosol, a cloud-clearing loop within SIBYL is applied to single-shot profiles at low altitudes as part of the layer detection algorithms to minimize cloud contamination of the aerosol. Because the backscatter signal from boundary layer cloud is usually much larger than the signal from the nearby aerosol, these clouds can be separated from aerosol based on backscatter intensity alone. To enhance the cloud–aerosol contrast, the cloud detection is done using 1064-nm profiles. The classification of all other layers is performed by the cloud–aerosol discrimination (CAD) algorithm (Liu et al. 2009).

CAD classifications are based on statistical differences in the various optical and physical properties of cloud and aerosol layers (Liu et al. 2004). Confidence functions constructed from the probability distribution functions (PDFs) of layer-averaged properties are used to discriminate between two classes: aerosols and clouds. For example, layer-averaged attenuated backscatter is generally larger for clouds than for aerosol, but strongly scattering aerosols and thin clouds can have similar backscatter magnitudes; in this case, the classification based on backscatter magnitude can be ambiguous. The ambiguity is reduced by simultaneous consideration of multiple parameters using multidimensional PDFs. Therefore, classification is based on a confidence function defined in terms of three-dimensional PDFs, which are based on layer averages of β'_{532}, attenuated total color ratio ($\chi' = \beta'_{1064}/\beta'_{532}$), and the midlayer altitude z. This three-dimensional test has been shown to perform better in discriminating aerosol and thin clouds in the upper troposphere than a two-dimensional algorithm based only on β' and z (Liu et al. 2004).

Because adjacent aerosol and cloud layers usually have significantly different backscatter intensity, aerosol and cloud layers are usually detected on different passes through SIBYL as separate homogeneous layers. Occasionally, however, a detected layer may include both cloud and aerosol. One example is broken clouds capping or embedded in dense dust layers, where the local backscatter intensity is well above the layer detection threshold despite the abrupt changes in layer type. The CAD algorithm is tuned to classify these mixed layers as cloud to avoid cloud contamination of the aerosol dataset.

Classifications for version 1 products were based on statistical models constructed using a limited set of observations from LITE and airborne lidars. For version 2, CALIOP observations were used to develop better models, providing improved classification performance.

2) Aerosol type and lidar ratio

After clouds are separated from aerosol layers, SCA attempts to identify the type of aerosol in the layer. By ''type,'' we mean a mixture of aerosol components that is characteristic of a region or an air mass. The mixture observed at a given location depends on local aerosol sources, wind trajectories and remote sources of aerosol, the state of internal and external mixing, chemical transformation processes that may have occurred during transport, and the state of hydration. An aerosol lidar ratio, $S_a = \sigma_a/\beta_a$, where σ_a is the aerosol extinction coefficient, is associated with each aerosol type so that identification of aerosol type provides a value of S_a to be used in the extinction retrieval. Aerosol type is also useful in its own right, because type identification is a step in the process of identification of the aerosol source and attribution of aerosol radiative forcing to natural or anthropogenic emissions.

We have adopted an observation-based approach to defining representative aerosol types, as opposed to a synthetic approach (e.g., Kahn et al. 2001). In the synthetic approach, models are defined for individual aerosol species, such as sulfate or sea salt, and mixtures of these components are used to represent observed aerosol types. However, these aerosol models involve assumptions on composition and mixing state and their representativeness can be questioned. The particular problem for application of the synthetic approach to lidar is that 180° backscatter tends to be sensitive to properties such as absorption, shape, and internal mixing state and to details of the size distribution, all of which are poorly known. Our approach assumes the variety of emission sources and atmospheric processes will act to produce air masses with typical identifiable aerosol characteristics. Our models are based on the use of remote sensing measurements to define and characterize these typical air masses. Each characteristic aerosol type is assumed to be a

TABLE 4. CALIPSO aerosol types and associated lidar ratios S_a.

Lidar ratio	Dust	Smoke	Clean continental	Polluted continental	Clean marine	Polluted dust
532 nm (sr)	40	70	35	70	20	65
1064 nm (sr)	30	40	30	30	45	30

mixture of aerosol species. Aerosol composition and characteristics will not be entirely homogeneous within the air mass, but this idealization allows a classification of aerosols that gives insight into the geographic distribution of aerosol types and provides constraints on the values of the aerosol lidar ratio required to relate aerosol extinction to backscatter in unconstrained retrievals of extinction.

Aerosol types were defined by performing a cluster analysis of aerosol parameters retrieved from the Aerosol Robotic Network (AERONET) sun-photometer network (Dubovik and King 2000). The analysis of AERONET retrievals yielded six distinct clusters, which were labeled desert dust, smoke, clean continental, polluted continental, clean marine, and polluted dust (Omar et al. 2005). The mean parameter values of each of these clusters defines an aerosol model from which S_a values at 532 and 1064 nm can be computed. For the clean-marine, clean-continental, and polluted-dust types, the models defined by the cluster means were adjusted to give 532-nm S_a values consistent with directly measured values (for details, see Omar et al. 2005). Measurements of 1064-nm S_a values are nearly nonexistent, so the lidar ratios at 1064 nm derived from this process are more uncertain than the 532-nm values. The smoke and polluted-continental cluster means yielded 532-nm S_a values consistent with measured values and were adopted without adjustment. Because of the sensitivity of 180° backscatter to particle shape, the 532-nm S_a value for the dust type was selected based on measured values and the aerosol model was selected from discrete dipole approximation (DDA) calculations using realistic assumptions on particle shape and composition (Kalashnikova and Sokolik 2002). The final aerosol lidar ratio values used in version 2 data processing are listed in Table 4.

The goal is to base typing decisions on the available ''lidar observables''—depolarization and two-wavelength backscatter—as much as possible and minimize the use of a priori assumptions. The typing algorithm is a decision tree that performs a number of tests using layer-averaged depolarization and 532-nm attenuated backscatter to attempt to identify aerosol as one of the six defined types (Omar et al. 2009). The depolarization ratio is used to discriminate aerosols containing dust from those primarily composed of hydrated droplets. The algorithm also makes some use of information on the altitude and geographic location of the aerosol layer and the surface type. In principle, CALIOP two-wavelength lidar signals allow the discrimination of small particles from large particles. However, χ' is not yet incorporated into the aerosol typing algorithm because the magnitude of χ' depends on both the backscatter color ratio and the extinction color ratio, which makes its interpretation ambiguous. Work in this area is in progress.

Once an aerosol type is determined, a lookup table is used to associate a lidar ratio with the aerosol type. Observed values of the aerosol lidar ratio range from 10 to 110 sr (Anderson et al. 2000), and a modeling study gives a somewhat smaller range of values (15–80 sr; Ackermann 1998). The goal of the aerosol typing algorithm is to classify the aerosol to constrain the uncertainty in lidar ratio to no more than 30%. When elevated aerosol layers are encountered with clear air underneath, S_a is computed directly from the integrated backscatter and layer transmittance (Young 1995). This derived value is used in place of the table value if the derived value has an uncertainty of less than 30%.

3) CLOUD ICE–WATER PHASE

The CALIOP laser transmits a pulse that is nearly 100% linearly polarized. The ratio of the perpendicular and parallel backscatter returns is the volume depolarization

$$\delta_V = \frac{\beta'_{\text{perp}}}{\beta'_{\text{par}}},$$

which provides an effective range-resolved way of determining whether the laser pulse has been scattered by liquid cloud droplets or by nonspherical ice crystals (Sassen 1991). It is well known that 180° backscatter from spherical particles retains the polarization of the incident light (van de Hulst 1957), whereas depolarization from cirrus is typically greater than 20% (Sassen and Benson 2001). This forms the basis of the CALIOP ice–water phase discrimination algorithm, and it is also key to the identification of the dust aerosol type.

There are complications in practice because of depolarization in dense water clouds from multiple scattering and because of signal noise in weaker layers. Depolarization from multiple scattering in water clouds can be related to the layer-integrated backscatter signal (Hu 2007) and tends to be lower than from ice clouds. The probability that a cloud is water or ice is computed based on the layer-averaged volume depolarization and the layer-integrated

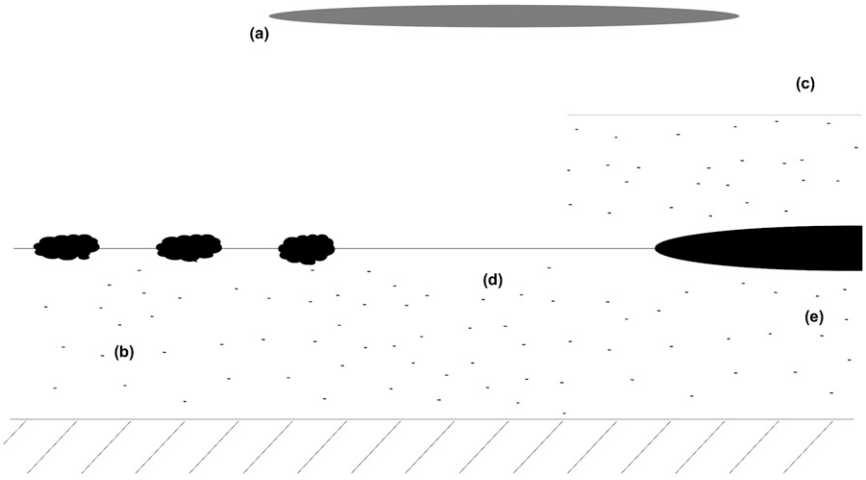

FIG. 5. Extinction retrieval scenarios: (a) isolated cirrus; (b) aerosol in clear sky or in clear columns between broken cloud; (c) aerosol above cloud; (d) aerosol below a higher layer (cloud or aerosol); and (e) aerosol beneath dense cloud.

backscatter signal, and it takes the depolarization SNR into account. This test provides a high-confidence classification much of the time. If the result of this test is ambiguous, a test based on the joint probability function of depolarization and cloud-top temperature is also applied.

Another complication is the possible presence of horizontally oriented planar ice crystals (Breon and Dubrulle 2004). Pulses from a near-nadir pointing lidar can be specularly reflected from these oriented planar crystals without significant depolarization. Clouds containing even small fractions of oriented crystals exhibit decreased depolarization and anomalously high backscatter (Sassen and Benson 2001). A simple empirical test has been included in the version 2 algorithms to identify clouds with obvious signatures of oriented crystals. In November 2007, the CALIOP nadir angle was increased from 0.3° to 3°, greatly reducing effects from oriented crystals. An improved ice–water phase algorithm has been developed which explicitly identifies oriented crystals (Hu et al. 2009) and will be implemented for a future data product release.

c. *Extinction retrieval*

HERA retrieves profiles of particle backscatter and extinction by using a simple iterative algorithm that has been found to be flexible and robust (Young and Vaughan 2009). The retrieval assumes a two-component atmosphere (molecules and particles). GMAO meteorological data define the properties of the molecular atmosphere. Solving for the unknown particulate extinction and backscatter requires either an a priori lidar ratio or the layer transmittance as a boundary condition. To generate the level 2 profile products, the retrieved profiles are averaged or replicated, as necessary, to a common resolution of 40 km horizontal and 120 m vertical for the aerosol profile product and replicated to 5 km horizontal and 60 m vertical for the cloud profile product.

HERA is designed to perform extinction retrievals by using results from the SIBYL and SCA algorithms, and it is designed with considerable flexibility because a variety of different scenarios must be considered. Several of the simpler ones are illustrated in Fig. 5. When the transmittance of a layer can be derived from the clear-air signal above and below the layer (Fig. 5a), it is used as a boundary condition on the retrieval (Young 1995). These constrained retrievals tend to be the most accurate retrievals, and this method also retrieves a representative value of the lidar ratio for the layer. When a transmittance measurement is not possible (e.g., boundary layer aerosol or opaque cloud), an a priori lidar ratio must be used. For aerosols, the lidar ratio comes from the SCA module. In version 2 processing, a constant value of 25 sr is used for ice clouds, which is the mean value measured by ground-based lidar (Sassen and Comstock 2001), and a constant value of 18 sr is used for water clouds.

As described above, boundary layer clouds and the region of atmosphere beneath them are identified and removed at single-shot resolution, allowing the retrieval of aerosols between broken clouds when the gaps between clouds are smaller than the required averaging interval (Fig. 5b). Aerosol detected above clouds when there is no cloud above the aerosol layer (Fig. 5c) is retrieved in the same way as in cloud-free conditions. When there are multiple layers—cirrus above boundary layer aerosol is a common situation (Fig. 5d)—the highest layer is retrieved first, allowing the signal below to be

corrected for the overlying attenuation. If there are more than two layers in the column, then the retrieved attenuation of all overlying layers is used for attenuation correction of the signal below. If the optical depth of the overlying layers is significant (Fig. 5e), then the required attenuation correction is large and the uncertainties in retrievals of the lower layers become large.

In version 2 data products, extinction retrievals are only performed on the layers detected by SIBYL. SNR in the clear regions above and between detected layers is low and extinction retrievals in these regions can result in the propagation of bias errors into detected layers having much larger SNR. However, the "clear air" regions may contain low levels of undetected aerosol. Regions with low concentrations of aerosol that are not detected or retrieved result in an underestimate of the column aerosol optical depth (AOD). Aerosol is harder to detect and can be missed if it is diffuse and spread throughout a deep column, especially if the lidar ratio is high, such as for smoke. Possibilities of retrieving and including these missing contributions to the column AOD will be explored for possible incorporation in a future data release.

The relatively large footprint size of space lidars can produce significant multiple scattering effects, which must be considered in the retrieval process. The priority in the development of the extinction retrieval algorithms was for the retrieval of extinction in aerosol layers and ice clouds. For CALIOP, multiple scattering effects in aerosol layers are generally small (and are currently neglected). Multiple scattering effects in ice clouds are significant but relatively easy to account for by using a constant that is independent of range and extinction (Winker 2003). Although extinction retrievals are performed on water clouds in the version 2 processing system, the appropriate multiple scattering corrections are not applied, which leads to large errors. Thus, in version 2 products, extinction and optical depth data for water clouds are unreliable and should not be used.

The algorithm provides a degree of constraint on the lidar ratio S, even for retrievals that are not constrained by a transmittance measurement. If the value of S that is supplied by SCA is too large, then the attenuation is overcorrected and the iterative solution may become unstable and divergent. In this case, S is automatically reduced until it is small enough to allow a nondiverging solution. If, on the other hand, the initial value of S is too small, then there will be insufficient correction for attenuation within the layer and the retrieved particulate backscatter can become negative. This is nonphysical and S is automatically adjusted to larger values until a nonnegative solution is achieved. These constraints on S become stronger as the layer optical depth increases,

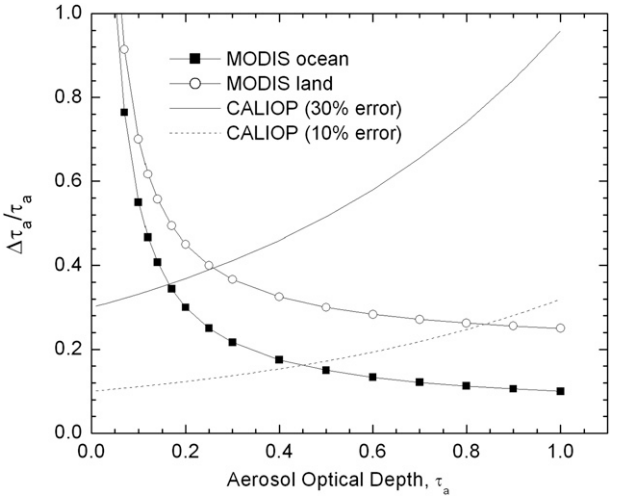

FIG. 6. Characteristics of AOD error for standard MODIS land and ocean aerosol retrieval algorithms and error in CALIOP AOD resulting from 10% and 30% errors in selection of lidar ratio S.

resulting in some degree of constraint on most cloud retrievals but the constraint only becomes effective on retrievals of the densest aerosol layers. When it is necessary to adjust S within the retrieval process to avoid a nonphysical retrieval, this is an indication that the initial value of S was inappropriate and the final retrieval results have large uncertainties. More details on the HERA lidar ratio adjustment scheme are provided in Young and Vaughan (2009).

For the highest layer in each column, the dominant error in unconstrained retrievals tends to be due to the choice of S. Calibration errors tend to be of lesser importance. To give some insight into the nature of the errors in unconstrained retrievals from HERA, an approximate expression for the optical depth error $\Delta\tau$ resulting from an error ΔS in lidar ratio is given by

$$\Delta\tau = \frac{0.5*(e^{2\tau} - 1)\Delta S}{S},$$

assuming enough averaging has been done that errors because of SNR are insignificant. For small optical depths, the relative error in optical depth is proportional to the relative error in lidar ratio: $\Delta\tau/\tau = \Delta S/S$. Figure 6 compares this error behavior with error estimates for the MODIS ocean and land aerosol retrieval algorithms (Tanré et al. 1997; Kaufman et al. 1997). For MODIS, relative AOD errors become large at small AOD, whereas for HERA the relative error increases with AOD and becomes very sensitive to uncertainties in S when AOD is greater than 1. Thus, CALIOP and MODIS are complementary in the sense that CALIOP is expected to be most accurate at low AODs, whereas

the MODIS retrievals tend to perform better at higher AODs. A rigorous error analysis of HERA retrievals has been developed and will be published in a future paper.

For columns containing multiple layers, incorrect values of S used in the upper layers cause errors in the transmittance corrections applied to the signal below, leading to errors in the retrieval of the underlying layers. These transmittance errors can be the dominant error source for underlying layers and retrievals of underlying layers are always more uncertain than if there were no layers overhead.

6. Summary and future directions

CALIOP represents a major advance in space-based active remote sensing of clouds and aerosols, and the CALIOP algorithms have many unique aspects designed to take advantage of these new capabilities. The approach of detection and retrieval at multiple spatial resolutions to optimize the trade-off between SNR and spatial resolution is new and unique to CALIPSO. Identification of aerosol type on a global scale from lidar observations is also being performed for the first time. The algorithms described here have been implemented in the CALIPSO production processing system and have been used to produce CALIPSO version 2 data. The production system has demonstrated its ability to process large volumes of lidar data; the version 2 dataset currently consists of over 19 TB of data representing 32 months of observations and 1.6 billion individual profiles.

A discussion of algorithm performance is beyond the scope of this paper, but a number of validation campaigns have been conducted and validation activities are ongoing. Although the algorithm development activity has had many successes, the algorithms are not yet fully mature. Experience gained from analysis of the data acquired by CALIOP has led to numerous improvements, and a variety of further algorithm improvement efforts are underway. New products are also in development, including cloud emissivity and particle size—derived using all three of the CALIPSO instruments—and products making use of A-train synergies such as radiative fluxes derived using CALIPSO, CERES, MODIS, and CloudSat.

Acknowledgments. The authors wish to acknowledge the support and successful cooperation of NASA and CNES, which made the CALIPSO mission possible.

REFERENCES

Abshire, J. B., X. Sun, H. Riris, J. M. Sirota, J. F. McGarry, S. Palm, D. Yi, and P. Liiva, 2005: Geoscience Laser Altimeter System (GLAS) on the ICESat Mission: On-orbit measurement performance. *Geophys. Res. Lett.,* **32,** L21S02, doi:10.1029/2005GL024028.

Ackermann, J., 1998: The extinction-to-backscatter ratio of tropospheric aerosol: A numerical study. *J. Atmos. Oceanic Technol.,* **15,** 1043–1050.

Anderson, T. L., S. J. Masonis, D. S. Covert, and R. J. Charlson, 2000: In situ measurements of the aerosol extinction-to-backscatter ratio at a polluted continental site. *J. Geophys. Res.,* **105,** 26 907–26 915.

Breon, F.-M., and B. Dubrulle, 2004: Horizontally oriented plates in clouds. *J. Atmos. Sci.,* **61,** 2888–2898.

Dubovik, O., and M. D. King, 2000: A flexible inversion algorithm for retrieval of aerosol optical properties from sun and sky radiance measurements. *J. Geophys. Res.,* **105,** 20 673–20 696.

Hahn, C. J., S. G. Warren, J. London, R. M. Chervin, and R. Jenne, 1990: Atlas of simultaneous occurrence of different cloud types over the ocean. NCAR Tech. Note TN-201+STR, 212 pp.

Hu, Y., 2007: Depolarization ratio–effective lidar ratio relation: Theoretical basis for space lidar cloud phase discrimination. *Geophys. Res. Lett,* **34,** L11812, doi:10.1029/2007GL029584.

——, and Coauthors, 2009: CALIPSO/CALIOP cloud phase discrimination algorithm. *J. Atmos. Oceanic Technol.,* **26,** 2293–2309.

Hunt, W. H., D. M. Winker, M. A. Vaughan, K. A. Powell, P. L. Lucker, and C. Weimer, 2009: CALIPSO lidar description and performance assessment. *J. Atmos. Oceanic Technol.,* **26,** 1214–1228.

Kahn, R., P. Banerjee, and D. McDonald, 2001: Sensitivity of multiangle imaging to natural mixtures of aerosols over ocean. *J. Geophys. Res.,* **106,** 18 219–18 238.

Kalashnikova, O. V., and I. N. Sokolik, 2002: Importance of shapes and compositions of wind-blown dust particles for remote sensing at solar wavelengths. *Geophys. Res. Lett.,* **29,** 1398, doi:10.1029/2002GL014947.

Kaufman, Y. J., D. Tanré, L. A. Remer, E. F. Vermote, A. Chu, and B. N. Holben, 1997: Operational remote sensing of tropospheric aerosol over land from EOS moderate resolution imaging spectroradiometer. *J. Geophys. Res.,* **102,** 17 051–17 067.

King, M. D., Y. J. Kaufman, D. Tanré, and T. Nakajima, 1999: Remote sensing of tropospheric aerosols from space: Past, present, and future. *Bull. Amer. Meteor. Soc.,* **80,** 2229–2259.

Liu, Z., M. A. Vaughan, D. M. Winker, C. A. Hostetler, L. R. Poole, D. Hlavka, W. Hart, and M. McGill, 2004: Use of probability distribution functions for discriminating between cloud and aerosol in lidar backscatter data. *J. Geophys. Res.,* **109,** D15202, doi:10.1029/2004JD004732.

——, and Coauthors, 2009: The CALIPSO lidar cloud and aerosol discrimination: Version 2 algorithm and initial assessment of performance. *J. Atmos. Oceanic Technol.,* **26,** 1198–1213.

McGill, M. J., D. Hlavka, W. Hart, V. S. Scott, J. Spinhirne, and B. Schmid, 2002: Cloud physics lidar: Instrument description and initial measurement results. *Appl. Opt.,* **41,** 3725–3734.

——, M. A. Vaughan, C. R. Trepte, W. D. Hart, D. L. Hlavka, D. M. Winker, and R. Kuehn, 2007: Airborne validation of spatial properties measured by the CALIPSO lidar. *J. Geophys. Res.,* **112,** D20201, doi:10.1029/2007JD008768.

Mishchenko, M. I., and Coauthors, 2007: Accurate monitoring of terrestrial aerosols and total solar irradiance: Introducing the Glory mission. *Bull. Amer. Meteor. Soc.,* **88,** 677–691.

Omar, A. H., J.-G. Won, D. M. Winker, S.-C. Yoon, O. Dubovik, and M. P. McCormick, 2005: Development of global aerosol models using cluster analysis of Aerosol Robotic Network (AERONET) measurements. *J. Geophys. Res.,* **110,** D10S14, doi:10.1029/2004JD004874.

——, and Coauthors, 2009: The CALIPSO automated aerosol classification and lidar ratio selection algorithm. *J. Atmos. Oceanic Technol.,* **26,** 1994–2014.

Powell, K. A., and Coauthors, 2009: CALIPSO lidar calibration algorithms. Part I: Nighttime 532-nm parallel channel and 532-nm perpendicular channel. *J. Atmos. Oceanic Technol.,* **26,** 2015–2033.

Russell, P. B., T. J. Swissler, and M. P. McCormick, 1979: Methodology for error analysis and simulation of lidar aerosol measurements. *Appl. Opt.,* **18,** 3783–3797.

Sassen, K., 1991: The polarization lidar technique for cloud research: A review and current assessment. *Bull. Amer. Meteor. Soc.,* **72,** 1848–1866.

——, and S. Benson, 2001: A midlatitude cirrus cloud climatology from the Facility for Atmospheric Remote Sensing. Part II: Microphysical properties derived from lidar depolarization. *J. Atmos. Sci.,* **58,** 2103–2112.

——, and J. M. Comstock, 2001: A midlatitude cirrus cloud climatology from the Facility for Atmospheric Remote Sensing. Part III: Radiative properties. *J. Atmos. Sci.,* **58,** 2113–2127.

Solomon, S., and Coauthors, 2007: Technical summary. *Climate Change 2007: The Physical Science Basis,* S. Solomon et al., Eds., Cambridge University Press, 19–91.

Stephens, G. L., and Coauthors, 2002: The CloudSat mission and the A-Train: A new dimension of space-based observations of clouds and precipitation. *Bull. Amer. Meteor. Soc.,* **83,** 1771–1790.

Tanré, D., Y. J. Kaufman, M. Herman, and S. Mattoo, 1997: Remote sensing of aerosol properties over oceans using the MODIS/ESO spectral radiances. *J. Geophys. Res.,* **102,** 16 971–16 988.

Thomason, L. W., M. C. Pitts, and D. M. Winker, 2007: CALIPSO observations of stratospheric aerosols: A preliminary assessment. *Atmos. Chem. Phys.,* **7,** 5283–5290.

van de Hulst, H. C., 1957: *Light Scattering by Small Particles*. Wiley and Sons, 470 pp.

Vaughan, M. A., S. A. Young, D. M. Winker, K. A. Powell, A. H. Omar, Z. Liu, Y. Hu, and C. A. Hostetler, 2004: Fully automated analysis of space-based lidar data: An overview of the CALIPSO retrieval algorithms and data products. *Laser Radar Techniques for Atmospheric Sensing,* U. N. Singh, Ed., International Society for Optical Engineering (SPIE Proceedings, Vol. 5575), 16–30.

——, M. J. McGill, Z. Liu, Y. Hu, R. E. Kuehn, and S. D. Rodier, 2008: Backscatter color ratios of cirrus clouds measured by the Cloud Physics Lidar. *Proc. 15th Int. Conf. on Clouds and Precipitation,* Cancun, Mexico, International Commission on Clouds and Precipitation, P13.16.

——, and Coauthors, 2009: Fully automated detection of cloud and aerosol layers in the CALIPSO lidar measurements. *J. Atmos. Oceanic Technol.,* **26,** 2034–2050.

Winker, D. M., 2003: Accounting for multiple scattering in retrievals from space lidar. *Lidar Scattering Experiments,* C. Werner, U. Oppel, and T. Rother, Eds., International Society for Optical Engineering (SPIE Proceedings, Vol. 5059), 128–139.

——, R. H. Couch, and P. McCormick, 1996: An overview of LITE: NASA's Lidar In-space Technology Experiment. *Proc. IEEE,* **84,** 164–180.

——, J. Pelon, and M. P. McCormick, 2003: The CALIPSO mission: Spaceborne lidar for observation of aerosols and clouds. *Lidar Remote Sensing for Industry and Environment Monitoring III,* U. N. Singh, T. Itabe, and Z. Lui, Eds., International Society for Optical Engineering (SPIE Proceedings, Vol. 4893), 1–11.

——, W. H. Hunt, and M. J. McGill, 2007: Initial performance assessment of CALIOP. *Geophys. Res. Lett.,* **34,** L19803, doi:10.1029/2007GL030135.

Young, S. A., 1995: Analysis of lidar backscatter profiles in optically thin clouds. *Appl. Opt.,* **34,** 7019–7031.

——, and M. A. Vaughan, 2009: The retrieval of profiles of particulate extinction from Cloud Aerosol Lidar Infrared Pathfinder Satellite Observations (CALIPSO) lidar data: Algorithm description. *J. Atmos. Oceanic Technol.,* **26,** 1105–1119.